Supplementary material for "Interannual variability of temperature in the UTLS region over Ganges-Brahmaputra-Meghna basin on COSMIC GNSS RO data"

Khandu
Department of Spatial Science
Curtin University, Perth Australia

Joseph L. Awange
Department of Spatial Science
Curtin University, Perth Australia

E. Forootan
Institute of Geodesy and Geoinformation
Bonn University, Bonn, Germany

December 6, 2015

1 Outline

This supplementary material contains information on the quality of radiosonde observations over the GBM river basin. Radiosonde stations are located mainly over India (18), China (3), and Bangladesh (3). The quality of radiosonde observations were assessed using collocated COSMIC RO profiles in the region and the results are briefly highlighted in the main document.

We have also briefly explained the geostatistial kriging method that is used to interpolate (grid) COSMIC RO data based on accumulated RO data over a month.

2 Radiosonde Data

COSMIC Data Analysis and Archive Center (CDAAC) also maintains radiosonde records from around the globe that are collocated with the RO profiles (e.g., COSMIC, CHAMP, GRACE). The radiosonde profiles are extracted from National Center for Atmospheric Research (NCAR) mass store, which is comprehensively described in *Sun et al.* (2010) including their sources and quality control procedures. There are 24 operational or synoptic radiosonde stations within or around the GBM basin, with most of them operated by the Indian Meteorological Department (IMD) (see, Figure 1). Three radiosonde stations are located in southern China (or the upper Brahmaputra basin), three are located in southern Bangladesh and the rest (18) of them are located inside the Indian territory. Based on the country of location, these radiosondes differ in their sensor types. The details of the radiosondes are provided in Table 1. The accuracy of IMD radiosondes have been a concern for many years due to their poor performance (see, e.g., *Das Gupta et al.*, 2005; *Kumar et al.*, 2011; *Sun et al.*, 2010; *Ansari et al.*, 2015) and has undergone major upgrades in the past 5-6 years.

A detailed evaluation of 12 sonde types globally by *Sun et al.* (2010) from April 2008 to October 2009 showed that IMD radiosondes performed poorly compared to COSMIC RO data while the Shang-E sondes from China suffered from large negative refractivity biases in the mid-troposphere. However, *Kumar et al.* (2011); *Ansari et al.* (2015) reported significant reduction in daily temperature fluctuations at 10 stations, which were prominent before they were upgraded. Therefore, improvements might be expected in humidity measurements. Collocated radiosonde profiles of temperature, water vapour pressure, and refractivity were extracted from CDAAC. There is a comprehensive discussion on the use of various collocation criteria for comparing radiosonde datasets and GNSS RO measurements in e.g., *Sun et al.* (2010), *Anthes* (2011), and *Khandu et al.* (2011). *Sun et al.* (2010) reported that collocation mismatches impacts the standard deviation errors by up to 0.35-0.42°C per 3 hours and 100 km respectively and ∼3% in specific humidity in the lower atmosphere. To maintain an optimum sample size, a collocation criteria of 200 km and 2-hour time difference was used to compare the radiosonde measurements and COSMIC profiles.

3 Comparison Methods

Radiosonde observations from within the GBM basin were compared with COSMIC RO profiles for the period August 2006 to December 2013. Mean differences ($\overline{\Delta X}$) and standard deviations (SD_X) of temperature (T) and water vapour pressure (p_w) between radiosondes and RO profiles at various pressure levels were computed as (e.g., *Sun et al.*, 2010):

$$\overline{\Delta X} = \frac{1}{n}\sum_{i=1}^{n}\left(X_i^R - X_i^C\right), \tag{1a}$$

$$SD_X = \sqrt{\frac{1}{n}\sum_{i=1}^{n}\left(\left(X_i^R - X_i^C\right) - \overline{\Delta X}\right)^2}, \tag{1b}$$

while for refractivity (N), the relative mean differences (Rel. $\overline{\Delta X}$) and standard deviations (Rel. SD_X) were computed as (e.g., *Sun et al.*, 2010):

$$\overline{\Delta X} = \frac{1}{n}\sum_{i=1}^{n}\left(\frac{X_i^R - X_i^C}{X_i^C}\right), \tag{2a}$$

$$SD_X = \sqrt{\frac{1}{n}\sum_{i=1}^{n}\left(\frac{\left(X_i^R - X_i^C\right)}{X_i^C} - \overline{\Delta X}\right)^2}, \tag{2b}$$

where X^R and X^C are the respective radiosonde and COSMIC temperature (T) or water vapour pressure (p_w) or refractivity (N), and $i = \{1, 2, ..., n\}$ at each pressure level for n data points.

4 Comparison of Radiosonde and COSMIC RO data

The quality of radiosonde types with respect to GNSS RO data has been reported in a number of studies (e.g., *Kuo et al.*, 2005; *Ho et al.*, 2009; *Sun et al.*, 2010, 2013; *Wang et al.*, 2013) and their overall agreement with COSMIC RO data has been found to be less than 0.15°C with a standard deviation

of 1.5-2.0°C (e.g., *Sun et al.*, 2010). In this section, the quality of different radiosondes across the GBM river basin (see, Table 1) were assessed using COSMIC RO profiles between August 2006 and December 2013. Of particular interest is the performance of the recently upgraded radiosondes at three stations in India: New-Delhi, Patna, and Dirbugarh, where major concerns were raised over the years (e.g., *Das Gupta et al.*, 2005; *Kumar et al.*, 2011; *Ansari et al.*, 2015). Statistical comparisons were made with respect to temperature, water vapour pressure, and refractivity using a collocation criteria of 200 km and 2 hours. While a more closer collocation criteria was deemed necessary for comparison due to drifts in radiosondes and tangent point horizontal drifts in GNSS RO data (*Sun et al.*, 2010; *Wang et al.*, 2013), the more relaxed criteria was used here considering the low number of samples at some stations such as those over Bangladesh and China. The number of collocated data points varied at each pressure level for both temperature and humidity (i.e., water vapour pressure) as most radiosondes tend to malfunction or burst out before reaching the lower stratosphere as shown in Figure 2.

[FIGURE 2 AROUND HERE.]

4.1 Temperature

Figure 3 shows the mean temperature difference and their standard deviations at 12 pressure levels from 850-30 hPa (or 1.5-24 km) of various radiosonde types against COSMIC RO data over the GBM basin. Their mean difference and standard deviations in the UTLS region are presented in Table 2. The quality of radiosondes differ highly among different sonde types with the closest agreement shown by ShangE indicating a mean difference of -0.06°C and a standard deviation of 1.44°C in the UTLS region (see, Table 2). The ShangM sonde showed a slightly larger (cold) bias between 400 hPa and 100 hPa (7.5-16.6 km) with an average standard deviation of around 2°C (Figure 3). Radiosonde observations (of two types) from 3 stations over Bangladesh indicated a large positive (warm) bias (>0.5°C) above 250 hPa (or 10.9 km) with standard deviations of more than 3°C (Figure 3). Their overall accuracy in the UTLS region was around 0.62-0.88°C with a standard deviation of 3.19-3.57°C (see, Table 2). Note that the number of RO data points vary along the vertical profile as radiosondes tend to burst out before reaching the lower stratosphere (Table 2). Their overall differences showed

relatively warmer biases in the lower atmosphere (below 200 hPa). However, they were usually cancelled out by cold bias in the upper regions (see Table 2). Other possible measures such as mean absolute deviation or root-mean-square errors can be used to represent bias error so that there will not be bias cancellation due to differing signs in bias at various altitude levels.

[FIGURE 3 AROUND HERE.]

On the other hand, the IMD-MK4 radiosondes showed anomalously large bias and standard deviations indicating both cold bias (up to 2.3°) in the upper troposphere (400-150 hPa; 7.5-14.2 km) and warm bias (up to 5°C) above 150 hPa (or 14.2 km) (see, Figure 3a). Their standard deviations ranges from 2°C-7°C from 850 hPa to 30 hPa (see, Figure 3b), which were consistent with the previous studies (e.g., *Sun et al.*, 2010; *Kumar et al.*, 2011; *Ansari et al.*, 2015). In order to see if there were any improvement at the three radiosonde stations (New Delhi, Patna, and Dilbugarh), a separate analysis was carried out using observations before (August 2006-May 2009) and after (June 2009-May 2013), i.e., the upgrading period. The analysis showed dismal improvement in temperature measurements (see, Figure 3) but showed a relatively smaller bias in the UTLS region with a mean difference of 1.2°C and a standard deviation of 4.1°C (see, Table 2). *Kumar et al.* (2011) reported that large diurnal temperature fluctuations found in previous observations were reduced significantly at the 10 upgraded stations across India. However, it should be noted that GPS receivers installed on radiosondes are designed to measure position (both horizontal and vertical) and speed (e.g., wind) and may have minimal impact on the temperature measurements.

[TABLE 2 AROUND HERE.]

4.2 Water Vapour

Water vapour plays an important role in the global and regional weather, climate, and hydrology but also is a major source of uncertainty in the lower troposphere contributing to about 3-4% of the error in observations in moist regions due to superrefraction and tracking errors (e.g., *Kuo et al.*, 2004; *Danzer et al.*, 2014). Water vapour pressure retrieved at CDAAC is based on the 1D-Var assimilation system that uses *a priori* information from

ECMWF, which also contains radiosonde observations and is hence not fully independent. Nevertheless, the IMD radiosonde observations were mostly not included in the ECMWF model (*Kumar et al.*, 2011), and could therefore highlight important differences against the COSMIC RO data. Figure 4 shows the mean difference and standard deviations of water vapour pressures from the radiosonde observations with respect to those from COSMIC RO data. All the radiosonde observations showed dry bias (of up to 30%) above 500 hPa (or 5.8 km) with respect to COSMIC RO data, with ShangE and ShangM indicating relatively larger biases than the rest of the sonde types (Figure 4a). However, radiosonde observations over Bangladesh and India (MK4) showed considerably wetter biases below 500 hPa. The standard deviation errors (Figure 4b) ranges from 0 in the upper troposphere (where water vapour is negligent) to more than 100% (or up to 3 hPa) at the near-surface at 850 hPa (1.5 km).

[FIGURE 4 AROUND HERE.]

4.3 Refractivity

Errors in refractivity are directly related to errors in observed temperatures and water vapour with the later contributing the most in the lower troposphere. The comparison results shown in Figure 5 indicated very large relative errors in IMD sondes (∼5%) corresponding to their very warm biases in the tropopause region (see, Figure 3a), while radiosonde observations over Bangladesh tend to show mean errors of less than 1% because of their relatively smaller biases. ShangE sonde showed the best performance above 300 hPa (or 9.6 km) indicating a relative bias of less than 0.25% while its counterparts ShangM sonde were also better than those from India and Bangladesh. The results of ShangE/ShangM sondes were consistent with the findings of *Sun et al.* (2010), which reported generally negative (0.3%) fractional errors in the lower troposphere and positive (0.1%) errors in the stratosphere (see, also, Table 2). The relative standard deviations of refractivity derived from various radiosonde types shown in Figure 5b largely resembles the standard deviation of the temperature difference (Figure 3b) ranging from about 5% (IMD) to less than 1% (ShangE/ShangM). Thus, very large refractivity errors in IMD sondes in the upper troposphere may have resulted from anomalously warm bias (see, Figure 3a) and possible errors in pressure measurements.

[FIGURE 5 AROUND HERE.]

5 Interpolation of COSMIC RO data

The ordinary kriging method uses a semi-variogram to characterize the spatial variability of the variable (Z) at a point of analysis grid (x_0). The unknown value $Z(x_0)$ is interpreted as a random variable located in x_0 and is the linear combination of observed values ($z_i = Z(x_i)$) and weights $\gamma_i(x_0)$ from neighbouring locations ($i = 1, ..., N$) obtained by (e.g., *Goovaerts*, 2000):

$$\hat{Z}(x_0) = \sum_{i=1}^{N} \gamma_i(x_0) \times Z(x_i), \qquad \text{where} \sum_{i=1}^{N} \gamma_i(x_0) = 1. \tag{3}$$

An experimental semi-variogram $\hat{\gamma}(h)$ is calculated for each month as (e.g., *Goovaerts*, 2000):

$$\hat{\gamma}(h) = \frac{1}{2N(h)} \sum_{i}^{N(h)} \left[Z(x_i) - Z(x_i + h) \right]^2, \tag{4}$$

where h is the distance between two points, $N(h)$ is the number of pairs separated by distance h, $Z(x_i)$ are the observed values at x_i, and $Z(x_i + h)$ are the observed values at the next point separated by h. A theoretical semi-variogram (e.g., gaussian, spherical, exponential, etc.,) is modelled to Equation 4 to minimise the error variance and to optimise smoothing. Figure 6 shows an example of three theoretical semi-variograms fitted to the experimental semi-variogram of COSMIC-derived tropopause temperature for September 2008. The tropopause temperature is rather spatially homogeneous over the GBM basin for September 2008 indicating a relatively homogenous surface until about 15° (or ∼1,500 km). This indicates the scale of the atmospheric variability as opposed to a complex terrain and its associate weather in the region. Based on our experiments we have adopted the spherical model for all the months.

[FIGURE 6 AROUND HERE.]

References

Ansari, M. I., R. Madan, and S. Bhaita (2015), Verification of quality of GPS based radiosonde data, *Mausam*, *66*(3), 367–374, available at: metnet.imd.gov.in/mausamdocs/16632_F.pdf.

192 Anthes, R. A. (2011), Exploring Earths atmosphere with radio occultation:
193 contributions to weather, climate and space weather, *Atmos. Meas. Tech.*,
194 *4*, 1077–1103, doi:10.5194/amt-4-1077-2011.

195 Danzer, J., U. Foelsche, B. Scherllin-Pirscher, and M. Schwärz (2014), Influ-
196 ence of changes in humidity on dry temperature in GPS RO climatologies,
197 *Atmos. Meas. Tech.*, *7*, 2883–2896, doi:10.5194/amt-7-2883-2014.

198 Das Gupta, M., S. Das, K. Prasanthi, and P. K. Pradhan (2005), Validation
199 of upper-air observations taken during the ARMEX-I and its impact on
200 the global analysis-forecast system, *MAUSAM*, *56*(1), 139–146.

201 Goovaerts, P. (2000), Geostatistical approaches for incorporating elevation
202 into the spatial interpolation of rainfall, *Journal of Hydrology*, *228*(1-2),
203 113129, doi:10.1016/S0022-1694(00)00144-X.

204 Ho, S. P., M. Goldberg, Y. H. Kuo, C. Z. Zou, and W. Schreiner (2009), Cali-
205 bration of temperature in the lower stratosphere from microwave measure-
206 ments using COSMIC radio occultation data: Preliminary results, *Terr.*
207 *Atmos. Oceanic Sci.*, *20*, doi:10.3319/TAO.2007.12.06.01(F3C).

208 Khandu, J. L. Awange, J. Wickert, T. Schmidt, M. A. Sharifi, B. Heck, and
209 K. Fleming (2011), GNSS remote sensing of the Australian tropopause,
210 *Climate Change*, *105*(3-4), 597–618, doi:10.1007/s10584-010-9894-6.

211 Kumar, G., R. Madan, K. Saikrishnan, S. K. Kundu, and P. K. Jain (2011),
212 Technical and operational characteristics of gps sounding system in the
213 upper air network of IMD, *Mausam*, *62*(3), 403–416, available at: metnet.
214 imd.gov.in/mausamdocs/16632_F.pdf.

215 Kuo, Y. H., T. K. Wee, S. Sokolovskiy, C. Rocken, W. Schreiner, D. Hunt,
216 and R. A. Anthes (2004), Inversion and error estimation of GPS radio
217 occultation data, *Journal of the Meteorological Society of Japan*, *82*(1B),
218 507–531, doi:10.1029/2004GL021443.

219 Kuo, Y.-H., W. S. Schreiner, J. Wang, D. L. Rossiter, and Y. Zhang (2005),
220 Comparison of GPS radio occultation soundings with radiosondes, *Geo-*
221 *physical Research Letters*, *32*(L05817), doi:10.1029/2004GL021443.

222 Sun, B., A. Reale, D. J., and D. C. Hunt (2010), Comparing radiosonde
223 and COSMIC atmospheric profile data to quantify differences among

radiosonde types and the effects of imperfect collocation on comparison statistics, *Journal of Geophysical Research*, *115*(D23), doi:10.1029/2010JD014457.

Sun, B., A. Reale, S. Schroeder, D. J. Seidel, and B. Ballish (2013), Toward improved corrections for radiation-induced biases in radiosonde temperature observations, *J. Geophys. Res.*, *115*, 42314243, doi:10.1002/jgrd.50369.

Wang, B. R., X. Y. Liu, and J. K. Wang (2013), Assessment of COSMIC radio occultation retrieval product using global radiosonde data, *Atmos. Meas. Tech.*, *6*, 1073–1083, doi:10.5194/amt-6-1073-2013.

Table 1: Details of various types of radiosondes used in and around the GBM river basin between August 2006 to December 2013. The upgraded IMD radiosondes were named as GPS (Global Positioning Sytem) sondes.

SL/No	WMO ID	Make	Location/Country	Latitude	Longitude	MSL [m]	# Profiles
1	42101	IMD MK4	PATIALA/INDIA	30°20'N	76°28'E	251	1354
2	42182	GPS Sonde	NEW DELHI/INDIA	28°35'N	77°12'E	216	2937
3	42314	GPS Sonde	DIBRUGARH/INDIA	27°29'N	95°1'E	111	1687
4	42339	IMD MK4	JODHPUR/INDIA	26°18'N	73°1'E	224	1142
5	42361	IMD MK4	GWALIOR/INDIA	26°14'N	78°15'E	207	245
6	42369	IMD MK4	LUCKNOW/INDIA	26°45'N	80°53'E	128	1244
7	42379	IMD MK4	GORAKHPUR/INDIA	26°45'N	83°22'E	77	864
8	42397	IMD MK4	SILIGURI/INDIA	26°40'N	88°22'E	123	432
9	42410	IMD MK4	GAUHATI/INDIA	26°6'N	91°35'E	54	810
10	42492	GPS Sonde	PATNA/INDIA	25°36'N	85°6'E	60	1066
11	42647	IMD MK4	AHMADABAD/INDIA	23°4'N	72°38'E	55	1366
12	42667	IMD MK4	BHOPAL/INDIA	23°17'N	77°21'E	523	1011
13	42701	IMD MK4	RANCHI/INDIA	23°19'N	85°19'E	652	1248
14	42724	IMD MK4	AGARTALA/INDIA	23°53'N	91°15'E	16	681
15	42809	IMD MK4	CALCUTTA/INDIA	22°39'N	88°27'E	6	2537
16	42867	IMD MK4	NAGPUR /INDIA	21°6'N	79°3'E	310	908
17	42874	IMD MK4	RAIPUR/INDIA	21°14'N	81°39'E	298	655
18	42971	IMD MK4	BHUBANESWAR/INDIA	20°15'N	85°50'E	46	1662
19	41923	VRS92G	DHAKA/BDESH	23°46'N	90°23'E	9	843
20	41977	Unknown	CHITTAGONG/BDESH	22°21'N	91°49'E	34	210
21	41883	Unknown	BOGRA/BDESH	24°51'N	89°22'E	20	21
22	56137	Shang/M	QAMDO/CHINA	31°9'N	97°10'E	3307	908
23	55591	Shang/E	LHASA/CHINA	29°40'N	91°8'E	3650	264
24	55299	Shang/E	NAGQU/CHINA	31°29'N	92°4'E	4508	2664

Table 2: Comparison of COSMIC RO data and observed soundings of different radiosondes used in and around the GBM river basin between August 2006 and December 2013. The number of collocated profiles slightly vary between temperatures and refractivities. The statistics were computed for the UTLS region (400-30 hPa) for temperatures and refractivities, and in the lower troposphere (850-200 hPa) for the water vapour pressures.

Radiosonde Types	ΔT (°C)	$\sigma\Delta T$ (°C)	Δp_w (hPa)	$\sigma\Delta p_w$ (hPa)	ΔN (%)	$\sigma\Delta N$ (%)	# Profiles (T/N)
unknown [Bdesh]	0.62	3.57	0.037	0.673	-0.32	1.37	161/161
Vaisala RS92 [Bdesh]	0.88	3.19	0.004	0.597	-0.42	1.11	134/134
MK4 [IMD]	2.77	4.97	0.058	0.090	-1.47	2.29	2292/2271
ShangE [China]	-0.06	1.44	-0.174	0.254	-0.26	0.88	657/657
ShangM [China]	-0.61	1.98	-0.186	0.193	0.02	1.05	247/247
Comparison between MK4 and GPS sondes at 3 stations in India							
MK4 [IMD]	2.72	4.01	-0.020	1.073	-1.39	1.88	271/270
GPS-sonde [IMD]	1.20	4.09	-0.142	0.686	-0.68	1.84	314/310

Table 3: Comparison of COSMIC RO data and observed soundings of different radiosondes used in and around the GBM river basin between August 2006 to December 2013. The number of collocated profiles slightly vary between temperature and refractivity. The temperature and refractivity statistics were computed for the UTLS region (400-30 hPa) and in the lower troposphere (850-200 hPa), the water vapour pressure statistics were computed.

Data	ΔT ($^{\circ}C$)	$\sigma\Delta T$ ($^{\circ}C$)	Δp_w **(hPa)**	$\sigma\Delta p_w$ **(hPa)**	ΔN (%)	$\sigma\Delta N$ (%)
Radiosonde	1.22	3.94	0.11	0.95	-0.64	1.83
ERA	0.15	0.99	0.07	0.41	-0.06	0.49
GFS	0.15	1.04	-0.01	0.47	-0.07	0.51

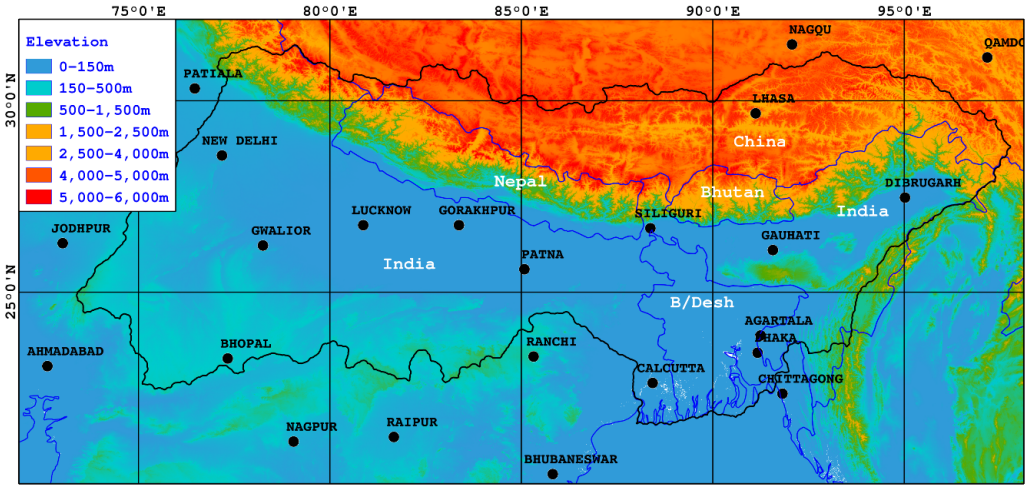

Figure 1: Elevation of the Ganges-Brahmaputra-Meghna Basin in South Asia. The digital elevation model is derived from the Shuttle Radar Topography mission (SRTM, http://srtm.csi.cgiar.org). The locations of the existing radiosonde stations are are shown in circles (black).

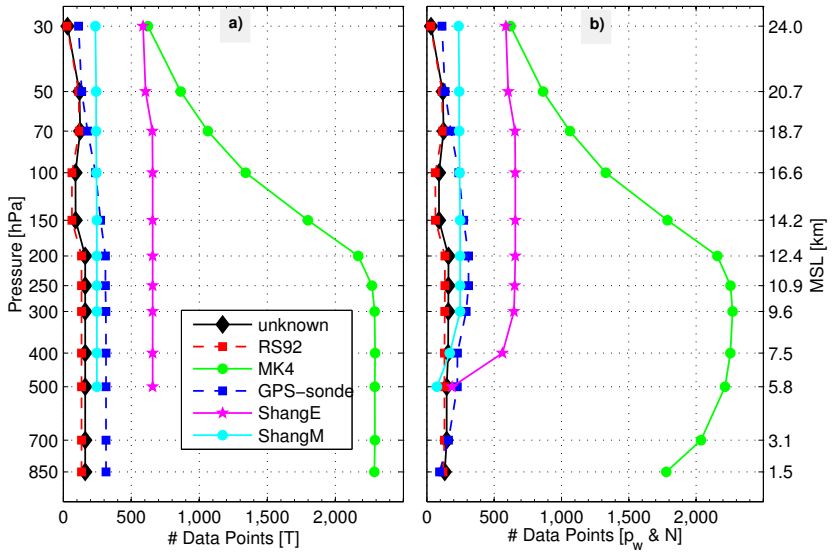

Figure 2: Number of data points at each pressure levels for temperature and humidity (water vapour pressure) of all the radiosonde types (see, Table 1) from August 2006 to December 2013.

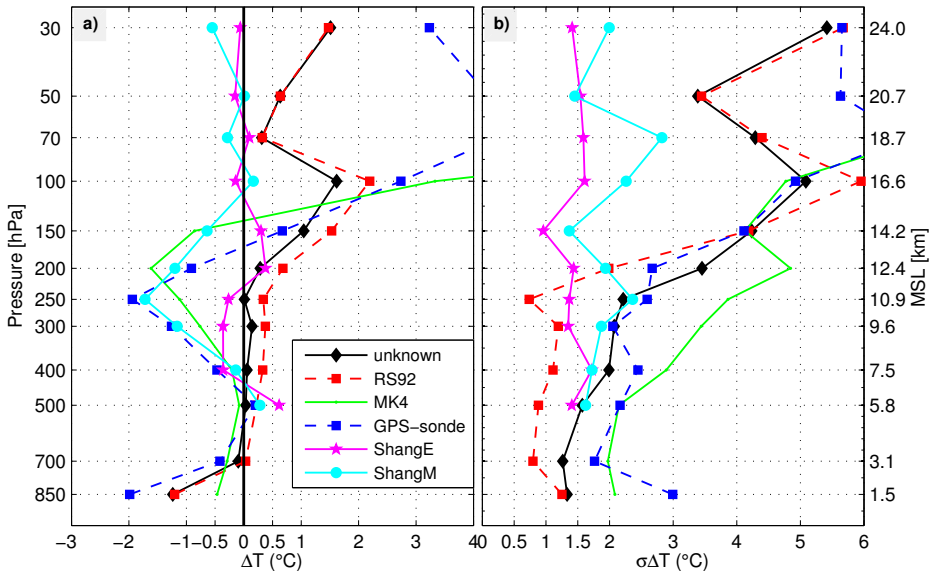

Figure 3: Mean temperature difference and standard deviations of various radiosonde types (refer to Table 1) with respect to COSMIC RO data over the GBM basin between August 2006 and December 2013.

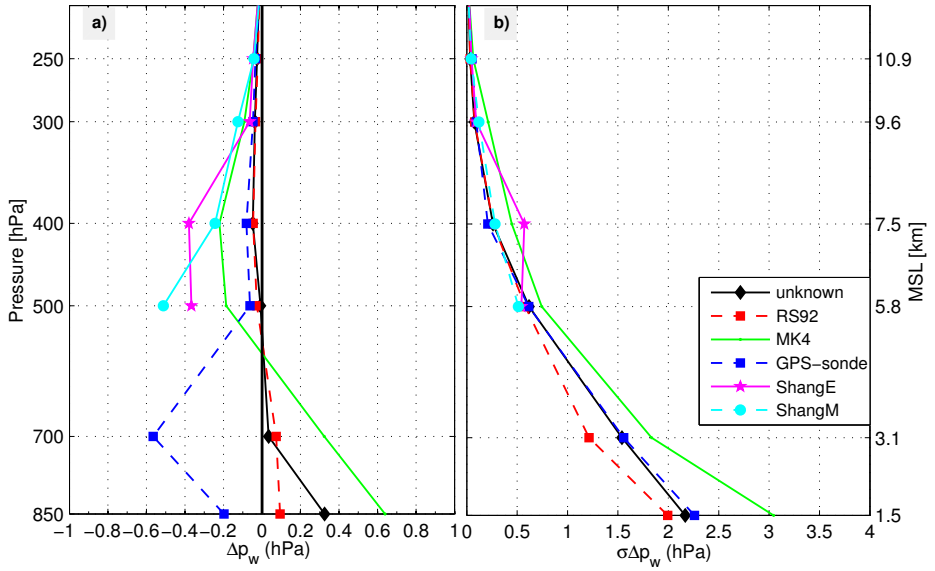

Figure 4: Mean differences and standard deviations of water vapour pressure (hPa) of various radiosonde types with respect to COSMIC RO data over the GBM basin between August 2006 and December 2013.

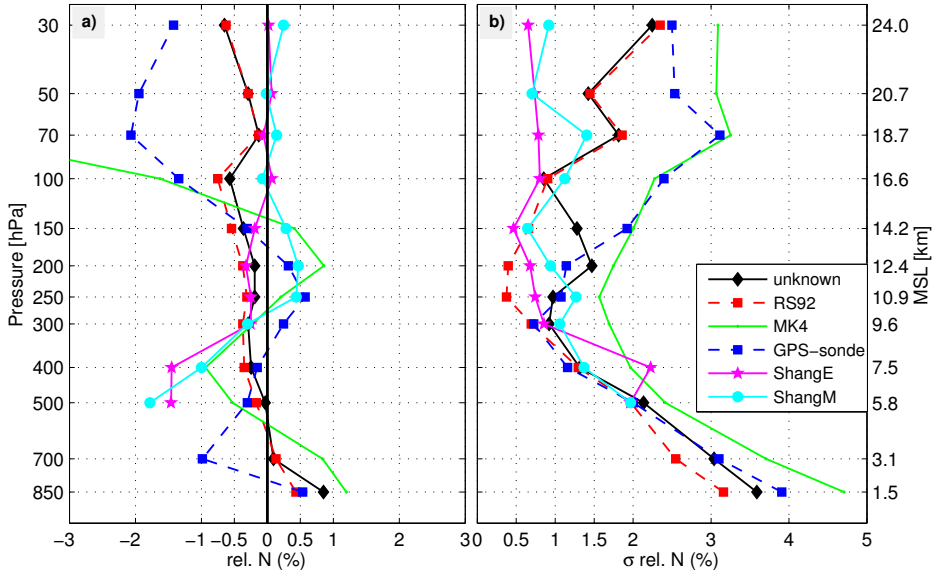

Figure 5: Relative mean differences and standard deviations of refractivity (in %) of various radiosonde types with respect to COSMIC RO data over the GBM basin between August 2006 and December 2013.

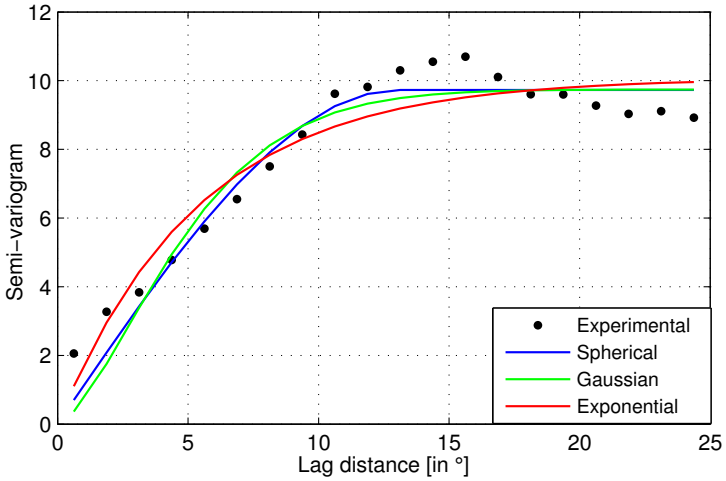

Figure 6: Semi-variogram of tropopause temperature (September 2008) over the GBM basin based on COSMIC RO data.